Research Article

Ibrahim Issah, Mohsin Habib and Humeyra Caglayan*

Long-range qubit entanglement via rolled-up zero-index waveguide

Abstract: Preservation of an entangled state in a quantum system is one of the major goals in quantum technological applications. However, entanglement can be quickly lost into dissipation when the effective interaction among the qubits becomes smaller compared to the noise-injection from the environment. Thus, a medium that can sustain the entanglement of distantly spaced qubits is essential for practical implementations. This work introduces the fabrication of a rolled-up zero-index waveguide which can serve as a unique reservoir for the long-range qubit–qubit entanglement. We also present the numerical evaluation of the concurrence (entanglement measure) via Ansys Lumerical FDTD simulations using the parameters determined experimentally. The calculations demonstrate the feasibility and supremacy of the experimental method. We develop and fabricate this novel structure using cost-effective self-rolling techniques. The results of this study redefine the range of light-matter interactions and show the potential of the rolled-up zero-index waveguides for various classical and quantum applications such as quantum communication, quantum information processing, and superradiance.

1 Introduction

Metamaterials are defined as artificially engineered structures with different material properties as compared to naturally existing materials [1, 2]. From their inception, these materials have played enormous roles in the manipulation

of electromagnetic fields in many disciplines [3, 4]. The unique properties of these materials have been identified to serve as means to enhance dipole-dipole interactions, energy harvesting, and long-range interactions of quantum emitters (i.e., quantum dots and diamonds (NV defect centers)) embedded within their waveguide-like meta-structures [5–8]. These physical systems find use in many quantum technologies such as quantum communication, quantum information processing [9], and single-photon generation [10, 11].

Other unique properties of metamaterials are related to the high enhancement of quantum emitter's response coupled with such a medium. These responses of emitters coupled to such an environment can be described by the dyadic Green's function which is related to the local density of states (LDOSs) formulations. This further leads to enhanced Purcell effects independent of the emitter position along and within the waveguide-like meta-structures. Experimental verifications of such material have been realized for a rectangular epsilon-near-zero (ENZ) waveguide using cathodoluminescence measurement techniques [12]. Fleury et al. [13] explored that the flexibility of dipole positions in ENZ waveguide channels at the cutoff wavelength is not the only relevance of these channels but could also boost Dicke superradiance effects which leads to a high collective coherent emission of the quantum emitters.

Plasmonic waveguide channels have also been identified to support extraordinary optical transmission when excited and have been implemented in the subwavelength regime to mediate long-range interactions of quantum emitters [14, 15]. Recently, Li et al. [16] presented a comparative study of ENZ and plasmonic waveguide channels used to enhance efficient long-range resonance energy transfer and inter-emitter entanglement. Although plasmonic waveguide types such as V-shaped grooves and cylindrical nanorods have been identified to outperform the sub-wavelength distance limitations of quantum emitters cooperative emission in a homogeneous medium, yet, quantum emitters entangled states mediated by these waveguides suffer from practical applications due to their dependence on the spatial position of emitters [14]. As

*Corresponding author: Humeyra Caglayan, Faculty of Engineering and Natural Science, Photonics, Tampere University, Tampere 33720, Finland, E-mail: humeyra.caglayan@tuni.fi. https://orcid.org/0000-0002-0656-614X
Ibrahim Issah and Mohsin Habib, Faculty of Engineering and Natural Science, Photonics, Tampere University, Tampere 33720, Finland. https://orcid.org/0000-0001-7663-4972 (I. Issah), https://orcid.org/0000-0002-6109-9468 (M. Habib)

a result, different techniques have been implemented by many authors to overcome these challenges [14, 16–18].

Note, due to the inherently short-range nature of the dipole-dipole interactions of quantum emitters in a homogeneous medium, it is relevant to identify different reservoirs that can be used to enhance the cooperative effects of quantum emitters [19]. The excitation of zero-index mode in such reservoirs makes it possible to enhance long-range interactions of quantum emitters as well as strong entanglement at farther distances. These waveguide channels, zero-index mode, exhibit a uniform field amplitude along the propagation axis which is independent of the axial dipole position due to the integrally large phase velocity [1, 20, 21].

These realizations of zero-index waveguide channels have intrigued much interest in the study of decay rate enhancement and cooperative emission of quantum emitters mediated by these channels [6]. Thereby, relevant to the practical realization of such zero-index waveguide channels with minimal constraints that can be used to enhance resonance energy transfer and long-range entanglement between two-level quantum fluorescence atoms (qubits) [22]. However, the difficulty to integrate quantum emitters in rectangular zero-index waveguide materials as well as the fabrication difficulties in the nanoscale regime has inhibited their practical applications [23]. To fulfill these zero-index features, the integration requires a controllable and feasible 3D fabrication process. The latter, while extremely pertinent from a fundamental perspective, poses limitations due to difficulties in sample fabrication, which may result in a reduced zero-index response or create a nonaccessible medium for integration and excitation of emitters.

Therefore, in this study, a self-assembled three-dimensional rolled-up zero-index waveguide will be our choice to overcome these deficiencies. We designed, fabricated, and numerically simulated, based on the parameters attained experimentally, alternating layers of metal and dielectric rolled-up zero-index waveguide to serve as an environment to mediate the cooperative emission of emitters embedded within it. We anticipate that the proposed rolled-up zero-index waveguide will enhance long-range dipole-dipole interactions and the preservation of entangled states due to its exotic properties to enhance super coupling within the cutoff region. To study these properties, we implemented the concept of rigorous dyadic Green's function relative to macroscopic quantum electrodynamics (QED) techniques to describe the response of a single fluorescence quantum emitter coupled to the rolled-up zero-index waveguide reservoir.

Also, we used the quantum master equation presented in the Supplementary section to numerically calculate the transient and steady-state entanglement between two-level atoms mediated by rolled-up zero-index waveguide using Wootters' concurrence formalism. Before the entanglement property calculations of the rolled-up zero-index waveguide, we first studied the photonic properties of the zero-index waveguide using Ansys Lumerical Finite Element EigenMode (FEEM) solver.

2 Zero-index waveguide modes

Ostensibly, long-distance entanglement between two quantum bits (qubits) is known to be mediated by photons. However, the recent emergence of the application of surface plasmons generation in different resonators and plasmonic waveguides has attracted researchers to delve into plasmon mediated entanglement between qubits in the nanoscale regime [13, 14]. This technique to confine optical fields in the subwavelength regime is fundamental in the application of surface plasmons in quantum optics. However, the sinusoidal phase change variations in propagating surface plasmon (SPP) mode of a waveguide channel limit the free distribution of quantum emitters in its corresponding environment [24]. It is thereby pertinent to use alternative means to examine other plasmonic channels with near-zero index properties and with the ability to enhance the entanglement of two qubits coupled with its excited zero-index waveguide mode.

Here, we investigate the fundamental TE_{11} mode of a rolled-up zero-index structure at the cutoff wavelength where there is minimal phase variation between two quantum emitters. Before investigating the fundamental mode, we examined the photonic properties of a traditional cylindrical hollow waveguide.

2.1 Cylindrical hollow waveguide

To serve as a guide to determine the fundamental mode of the rolled-up zero-index waveguide composed of an alternating layer of metal and dielectric, we numerically implement the analytical equation for a homogeneous circular waveguide with an air core [25]. The dispersion relation of the rolled-up zero-index waveguide is initially calculated to identify the cutoff wavelength, where the propagation constant $k = 0$. At this wavelength, the electromagnetic waves can be squeezed or tunneled through a waveguide to exhibit a similar response as zero-index materials. This phenomenon relative to circular waveguides has been

demonstrated theoretically by Pan et al. [26] to exhibit unique electromagnetic tunneling which is independent of the waveguide length.

From the Helmholtz eigenvalue equation, the cutoff wavelength as a function of the effective mode index of a circular hollow waveguide can be expressed analytically as

$$n_{\text{eff}} = \sqrt{1 - \left(\frac{u_{nm}}{\pi}\right)^2 \left(\frac{\lambda}{2\rho}\right)^2}, \tag{1}$$

where n_{eff} is the effective index as a function of dielectric core diameter, u_{nm} is the root of the Bessel function, ρ is the radius of the circular core, and λ is the wavelength. Since our mode of interest is the fundamental TE_{11} mode, the corresponding root of the Bessel function selected is 3.832. The analytical calculation of the dispersion relation of a cylindrical dielectric waveguide is shown in Figure 1(a). This served as a benchmark to determine the

cutoff frequency of the rolled-up zero-index waveguide presented in Figure 1(b) for different diameters D.

For different core diameters D of both the cylindrical and zero-index hollow waveguides, we obtained a redshift of the cutoff wavelength. This shows the dependence of the cutoff wavelength on the material dimensions. The dispersion of the cylindrical hollow metallic (i.e., gold (Au)) waveguide (dotted lines) superimposed on Figure 1(b) shows a similar dispersion relation as the rolled-up zero-index waveguide. Figure 1(c) illustrates the unique and complex modes of the rolled-up zero-index waveguide at different effective indices (n_{eff}). The complex mode profiles with effective cladding index ($n_{\text{eff}} \neq 0$) are mostly confined in the metal-dielectric cladding region due to the excitation of plasmon modes. However, the fundamental mode of the waveguide with $n_{\text{eff}} \simeq 0$ confined in the core possesses a similar dispersion relation with the fundamental
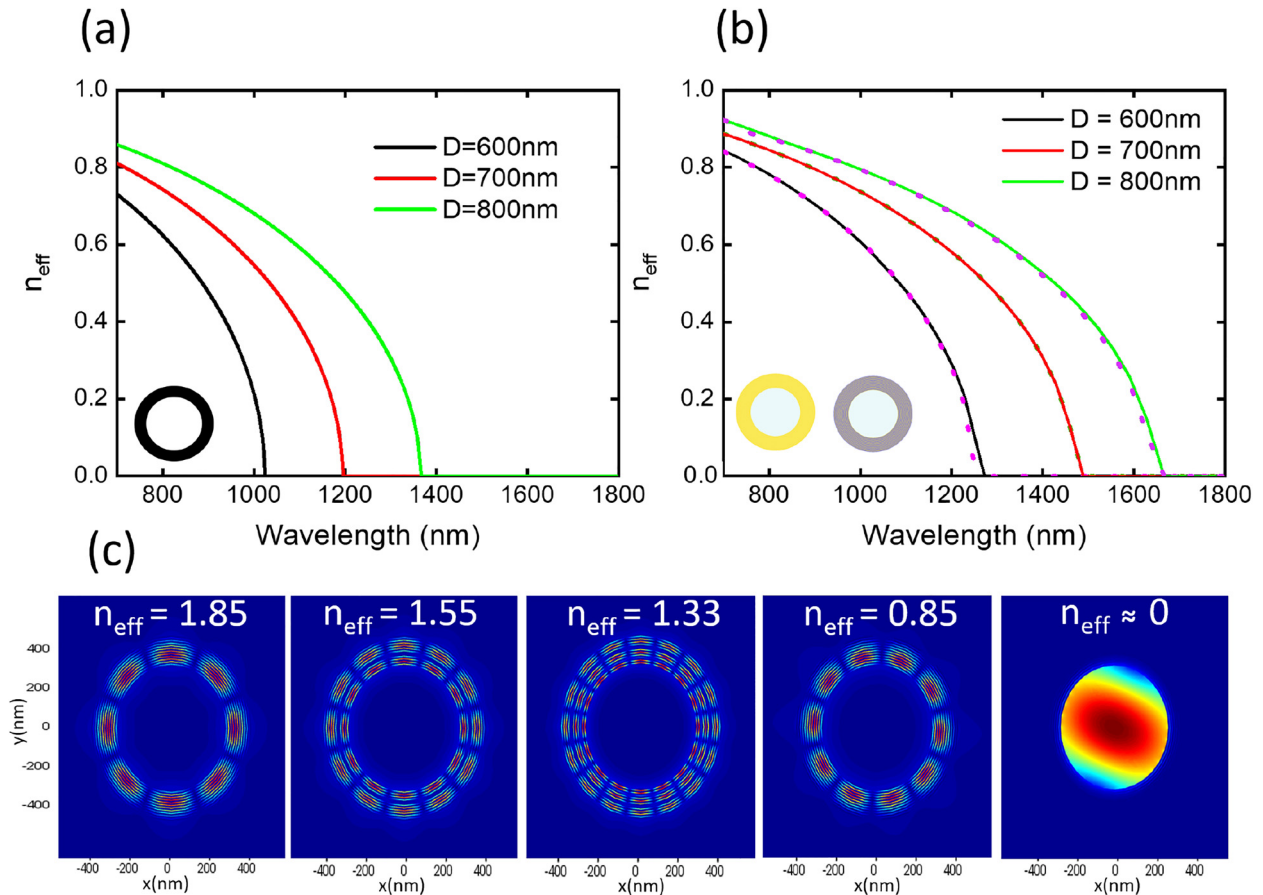

Figure 1: Photonic properties of a cylindrical hollow waveguide and a rolled-up zero-index waveguide with its corresponding mode profiles. (a) The dispersion relation of a cylindrical hollow waveguide with different core diameters D. The schematic of the homogeneous circular waveguide is represented by the black circular inset. (b) The dispersion relation of the rolled-up zero-index waveguide (solid lines). The dotted lines in the same figure show similar dispersion calculated for the cylindrical hollow metallic waveguide. The yellow circular inset represents the cylindrical hollow metallic waveguide and the rolled-up tube is represented by the multilayer gray circular inset. The cutoff wavelength varies as a function of the core diameter D in both figures (top panel). (c) The different mode profiles excited in the rolled-up zero-index waveguide ($D = 700$ nm) for different effective indices (n_{eff}) with $n_{\text{eff}} \simeq 0$ depicting the fundamental TE_{11} mode.

modes of the plasmonic hollow waveguide. This waveguide fundamental mode with an effective index near zero introduces novel ways of controlling optical field propagation and enhancement due to the infinite phase velocity of the tunneled electromagnetic wave.

2.2 Rolled-up zero-index waveguide

In this section, we described how the proposed structure can be fabricated.

The first rolled-up tubes were fabricated by Prinz et al. using strained InAs/GaAs bilayer with lattice mismatch [27]. The layers start to roll as the sacrificial layer beneath them is released by an etchant. However, semiconductor-based rolled-up tubes are not suitable for our purpose, due to the high refractive indices of materials as compared to near-zero refractive index material required for this study. In this study, we adopted a similar strained induced self-rolling mechanism to obtain a three-dimensional rolled-up zero-index waveguide of Au and SiO_2 on a silicon (Si) substrate using germanium (Ge) as a sacrificial layer (see Supplementary for details). Figure 2(a) illustrates the schematics of the proposed design. Figure 2(b) depicts the scanning electron microscope (SEM) image of the fabricated rolled-up zero-index waveguide. The structure has a
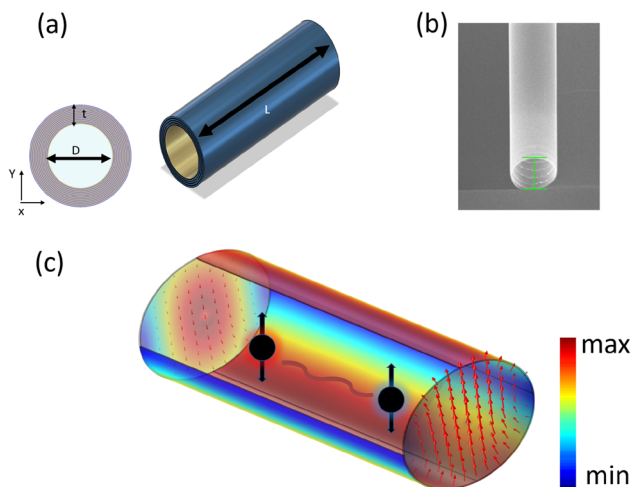
Figure 2: Rolled-up zero-index waveguide schematics and fabricated sample.
(a) Schematic of the rolled-up zero-index waveguide (b) SEM images of the fabricated waveguide. The green line corresponds to a diameter of 700 nm and the length of the waveguide is 25 μm. (c) The volumetric display of the normalized fundamental TE_{11} mode propagation in the rolled-up zero-index waveguide. The embedded dipoles (qubits) are denoted by the black spheres with arrows. The interaction between the dipoles mediated by the zero-index mode is represented by the curvy lines. The surface vector plot shows the field distribution of the fundamental mode.

core diameter (D) of 700 nm, consisting of 12 alternating bi-layers, 10 nm of Au and 5 nm of glass silica (SiO_2) thick, and length (L) of 25 μm.

The benefit of the rolled-up zero-index waveguide over other plasmonic waveguide channels is that it offers different emitters integration techniques into the core of the waveguide. For example, injection techniques of colloidal nanoemitters using microsyringe technique. In such a case, the driving of nanoemitters is mediated by capillary forces [28]. Another method of integrating quantum emitters to the core of the rolled-up zero-index waveguide is to deposit emitters on the planar bilayer before initiating the rolling process.

We now move to the numerical calculations based on the parameters of the fabricated structure. However, due to the existence of the nonradiative and propagation losses, the 25 μm length of the fabricated waveguide is approximated to be 3 μm in the simulation. Moreover, the 3 μm was identified to suffice for determining the coupling parameters of an emitter positioned at the central part of the rolled-up zero-index waveguide. It is worth noting that the numerical calculation suggests that for a dipole placed at the central part of the waveguide, its decay rate vanishes beyond 3 μm as we shall see in Figure 4.

The core diameter of the rolled-up structure is filled with a material permittivity of one. Material dispersion of Au from Johnson and Christy [29] material dispersion data and Palik [30] data for the SiO_2 layers were used in the modeling. Figure 2(c) also shows the volumetric display of the fundamental mode of the rolled-up zero-index waveguide at the cutoff wavelength $\lambda \simeq 1450$ nm. The embedded dipoles represent the quantum emitters mediated by the zero-index mode of the rolled-up zero-index waveguide, and the vector surface plot shows the field distribution of the fundamental TE_{11} mode. Note that in the case of the fundamental TE_{11} mode both radial and axial components of the transverse fields exist resulting in the distribution of total electric and magnetic field in the rolled-up zero-index waveguide cross-section.

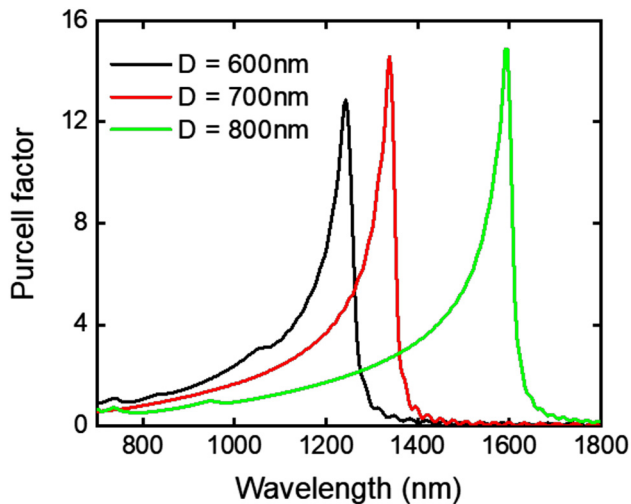# 3 Decay rate enhancement of the rolled-up waveguide

As stated initially, advances in plasmonic materials (i.e., V-shaped grooves, cylindrical nanorods) and ENZ plasmonic metamaterials (i.e., plasmonic planar waveguide) have availed the opportunity to enhance superradiant effects of a collective quantum emitter which outperforms the weak interaction of emitters in a homogeneous medium [13].

The superradiance effect known as the collective effect of quantum emitters arranged close to each other was proposed by Dicke [31] to show the relationship between the radiation intensity of quantum emitters and the number of quantum sources. This radiant effect is linked to the exotic properties of the reservoir to which the quantum emitters are coupled to.

At the cutoff wavelength region of the rolled-up zero-index waveguide channel, we foresee a high LDOS of the quantum emitter embedded in the waveguide structure. This enhancement at the cutoff wavelength is insensitive to the emitter axial position and thereby exhibits the aforementioned inherent flexibility of emitters position in zero-index metamaterials [16, 32, 33].

To verify the high LDOS at the cutoff wavelength, we computed the Purcell factor of the proposed rolled-up zero-index waveguide channels as a function of different waveguide core diameters D. Figure 3 presents the corresponding Purcell factor calculation. It can be seen that the spectral resonance response of a single quantum emitter coupled to a rolled-up zero-index waveguide is dependent on the core diameter D. As the diameter increases the spectral density response redshifts to a higher wavelength similar to the dispersion relation in Figure 1(b). For the waveguide channel with a core diameter of $D = 700$ nm, the peak enhancement is around the cutoff wavelength (i.e., $\lambda \simeq 1450$ nm).

Above the cutoff wavelength, the decay rate is predominantly quenched by the environment as there is a very low density of states due to the quenched propagating modes in the waveguide. However, below the cutoff wavelength, there is monotonic build-up in the decay rate

reaching a maximum at the cutoff wavelength. Close to the cutoff wavelength, the decay rate is not only enhanced but remains uniform along the waveguide channel. This uniformity is due to the nonresonant mode distribution at the cutoff wavelength [12].

4 Rolled-up zero-index waveguide dipole-dipole coupling and decay rate

To determine the key parameters (i.e., decay rate (γ_{12}) and dipole-dipole coupling ($\pm g_{12}$)) to solve the quantum master equation in Eq. (S3), we calculate the γ_{12} and $\pm g_{12}$ of an emitter embedded within the rolled-up zero-index waveguide using the dyadic Green's function obtained from FDTD simulations (see Supplementary for details). We study these parameters of the quantum master equation at three different wavelengths (i.e., the cutoff wavelength ($\lambda = 1450$ nm) and at two other wavelengths: close ($\lambda = 1300$ nm) and far ($\lambda = 1250$ nm) from the cutoff wavelength).

Figure 4(a) depicts the dipole-dipole interactions of quantum emitters embedded in the rolled-up zero-index waveguide at three different wavelengths as a function of interatomic distance (r_{12}/λ_0). At the cutoff wavelength, the dipole interactions increase appreciably at short-range and decay exponentially as a function of interatomic distance as compared to the other two wavelengths. At $\lambda = 1250$ nm and $\lambda = 1300$ nm, we identified an oscillatory behavior of the dipole-interactions as compared to the cutoff wavelength. This oscillatory behavior of the two wavelengths relative to the cutoff wavelength is also shown in the spontaneous decay rate of the quantum emitter as shown in Figure 4(b). Figure 4(c)–(e) presents the energy transfer resonance, which is dependent on the dyadic Green's function of the qubits inside the rolled-up zero-index waveguide [34]. This shows that, at the cutoff wavelength, the rolled-up zero-index waveguide provides modes with a longer wavelength and minimal phase variations to enhance strong entanglements of two qubits placed at farther distances.

At the cutoff wavelength $\lambda_0 = 1450$ nm, we also see a long-range decay rate as a function of interatomic distance which enhances qubit entanglement. It is evident that the comparison between the normalized decay rate and the dipole-dipole interaction at the cutoff wavelength satisfies the condition of attaining high entanglement

Figure 3: Decay rate enhancement for different core diameters D of the rolled-up zero-index waveguide.
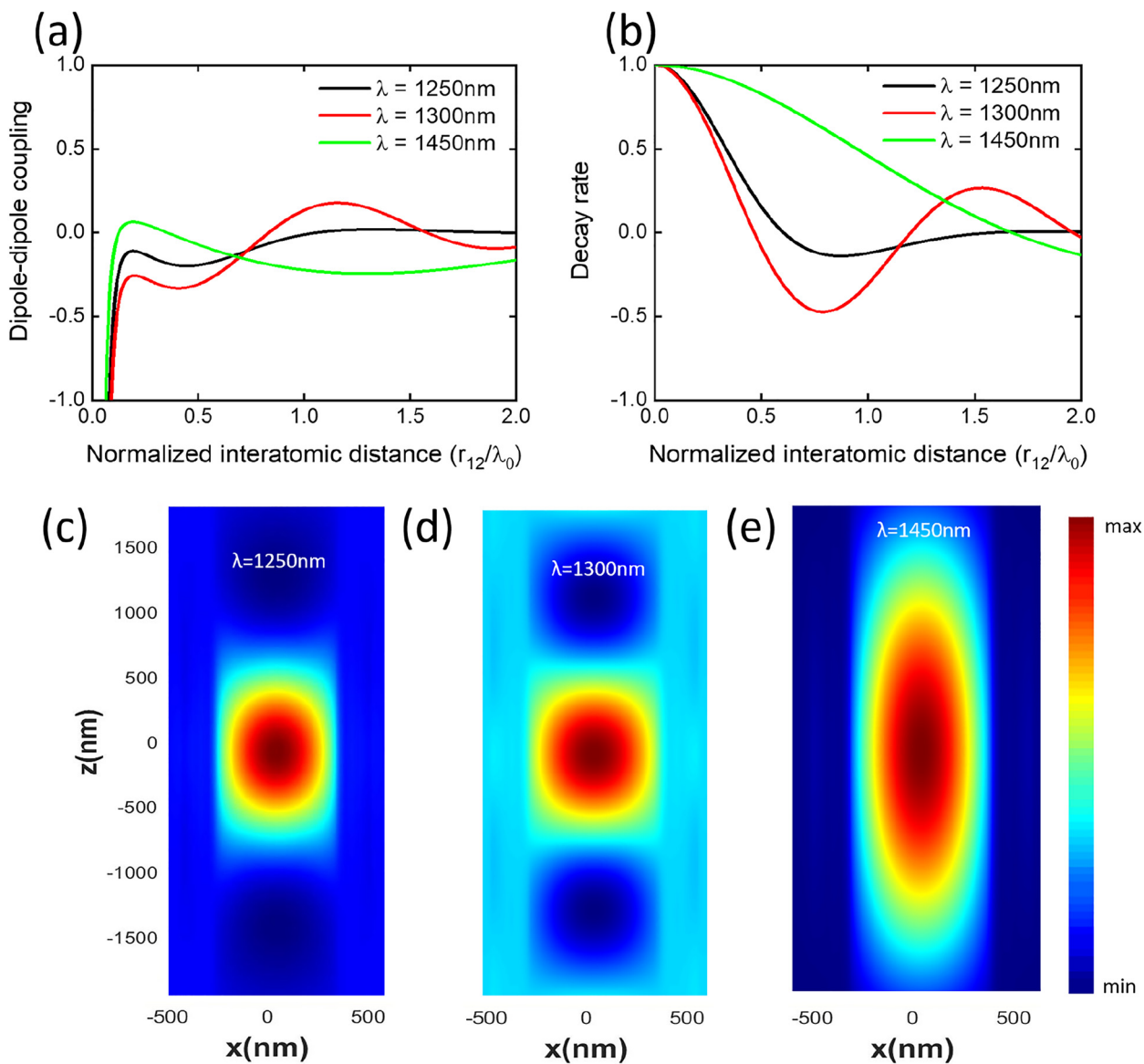
Figure 4: Coupling parameters of the rolled-up zero-index waveguide.
(a) The dipole-dipole interaction and (b) the decay rate of emitters coupled to the rolled-up zero-index waveguide at different excitation wavelengths. Energy transfer resonance (ETR) of the rolled-up zero-index waveguide for the different excitation wavelengths: (c) 1250 nm, (d) 1300 nm, and (e) 1450 nm.

performance i.e., $g_{12} \ll \gamma$ and $\gamma = \gamma_{12}$ as shown in Figure 4(a) and (b). Note that the emitter's decay time at the cutoff wavelength is normalized by its maximum value of approximately 10^{-5} s at normalized interatomic distance $r_{12}/\lambda_0 = 0$. The maximum value of the decay time is represented by the qubit self-interaction term γ. We also observed that $r_{12}/\lambda_0 = 0$ to $r_{12}/\lambda_0 = 1$, there is an appreciable high decay ratio γ_{12}/γ which results in a suppression of the subradiant decay state $|-\rangle$ as compared to the superradiant $|+\rangle$ state (i.e., superradiant $\gamma + \gamma_{12}$ and subradiant

$\gamma - \gamma_{12}$ decay rates) (see Supplementary for details). Based on the coupling parameters (Figure 4(a) and (b)) and energy transfer resonance (Figure 4(e)) predicts strong long-range interaction of qubits and high persistence of entangled states in the rolled-up zero-index waveguide at the cutoff wavelength.
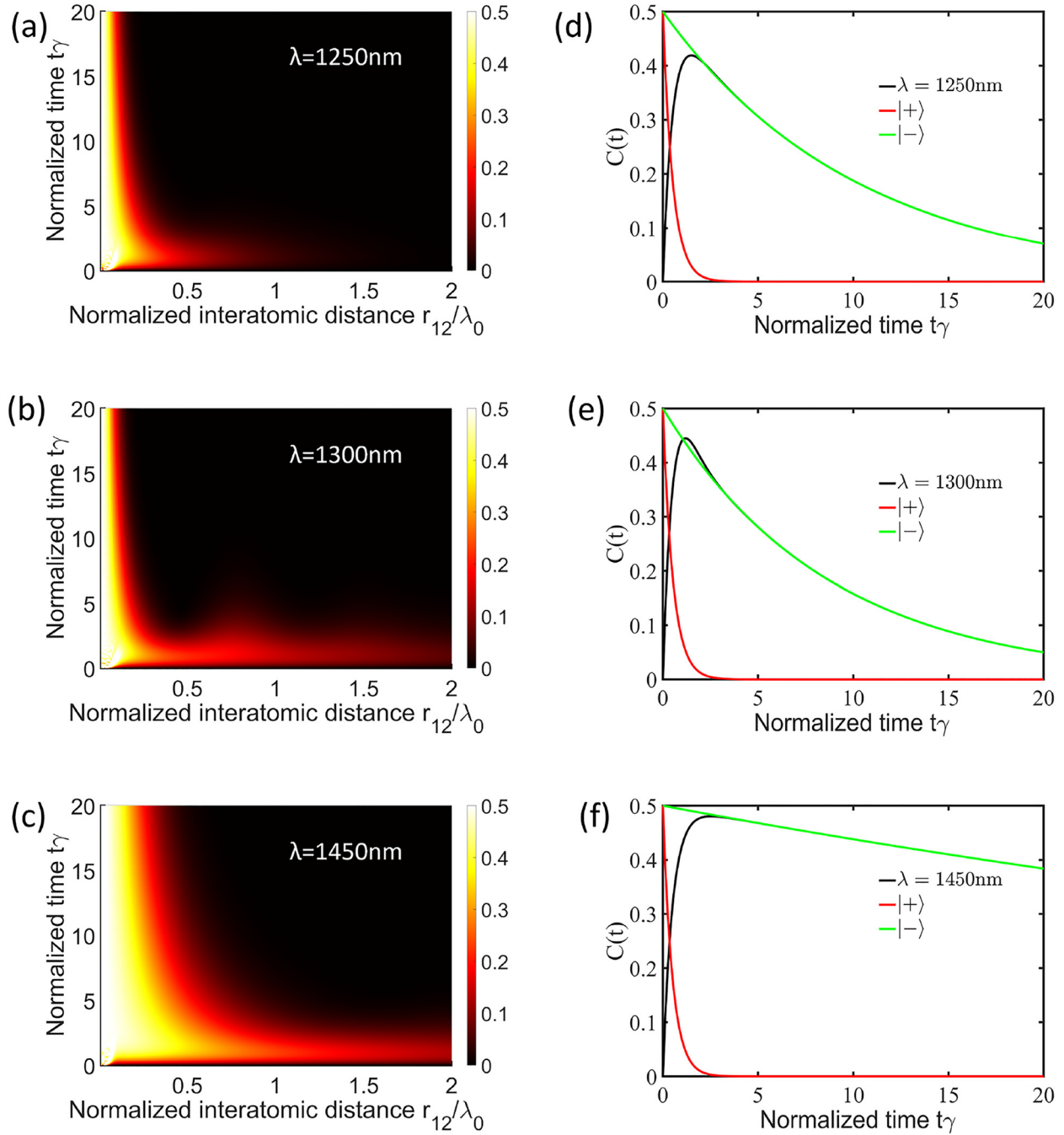
4.1 Measure of entanglement

Using the decay rate (γ_{12}) and the dipole-dipole interactions $(\pm g_{12})$ of the qubits inside the rolled-up

zero-index waveguide, we calculated the corresponding concurrence metric measure of entanglement (transient and steady-state) using Eqs. (S8) and (S9) (see Supplementary for details). This measure of entanglement is relevant to determine the long-range interactions of quantum emitters and their duration.

4.1.1 Transient entanglement mediated by rolled-up zero-index waveguide

Using the cutoff wavelength λ_0 and self-interactions γ as a normalization factor for both the interatomic distance r_{12}, and evolution time t, we calculated the concurrence metric of the quantum emitters as a function of normalized time

Figure 5: The measure of entanglement between qubits embedded within the rolled-up zero-index waveguide.
(a)–(c) The concurrence metric heatmap for different wavelengths: (a) 1250 nm, (b) 1300 nm, and (c) 1450 nm (zero-index wavelength). (d) and (e) Similar concurrence metric plot at normalized interatomic distance ($r_{12}/\lambda_0 = 0.1$) and their corresponding symmetric $|+\rangle$ and antisymmetric $|-\rangle$ states.

γt and interatomic distance r_{12}/λ_0 at different wavelengths using Eq. (S8) (see Supplementary for details).

Figure 5(a)–(c) illustrates the measure of entangled states using the concurrence metric formalism for the different wavelengths. It is evident that the concurrence metric is higher at the cutoff wavelength as compared to the other two wavelengths. The high concurrence as a function of time and inter-emitter distance is due to the excitation of the zero-index mode of the waveguide which mediates the long-range interactions of the quantum emitters. At $\lambda = 1300$ nm, which is closer to the cutoff wavelength ($\lambda = 1450$ nm), shows a higher entanglement as compared to the concurrence for $\lambda = 1250$ nm.

The excited mode at $\lambda = 1250$ nm wavelength region has efficient entanglement at short-range but decreases monotonically as a function of inter-emitter distance due to the confined field as shown in Figure 4(c). However, at the cutoff wavelength, we obtain a large homogeneous electromagnetic field as shown in Figure 4(e). This results in a large decay rate value and small dipole-dipole interactions and thereby leads to a higher concurrence independent of the emitter position. To appreciate the latter effect, we plotted the concurrence metric at $r_{12}/\lambda_0 = 0.1$ as a function of normalized time γt for the different wavelengths, i.e., $\lambda = 1250$ nm, $\lambda = 1300$ nm, and $\lambda_0 = 1450$ nm, respectively, as shown in Figure 5(d), (e), and (f). It is clear that at the cutoff wavelength, we have high concurrence which persists for an appreciable time as compared to the other wavelengths. This effect is a consequence of the suppressed subradiant state $|-\rangle$ as compared with the high superradiant $|+\rangle$ decay channels which are superimposed on the concurrence plot in Figure 5(d)–(f). Clearly, a decrease in the population dynamics of the subradiant state $|-\rangle$ at $\lambda = 1250$ nm and $\lambda = 1300$ nm wavelengths results in a lower persistence of entanglement over time. Comparatively, the dependence of the subradiant $|-\rangle$ population of states is appreciably high at the cutoff wavelength which leads to a high concurrence state.

### 4.1.2 Steady-state entanglement mediated by rolled-up zero-index waveguide

Up until now, we have justified the relevance of concurrence metric key parameters (i.e., γ_{12}, $\pm g_{12}$) which can be beneficial to achieve appreciable entanglement useful for quantum information processing and communication. We have also demonstrated the concurrence as a function of normalized time and interatomic distance as well as illustrate the flexibility of emitter axial positions at the cutoff wavelength for the rolled-up

zero-index waveguide. However, this entanglement decays with time as shown in Figure 5(d)–(f). In the case of Figure 5(f), we can visualize the reduction in concurrence as a function of the gradual monotonic decay of the subradiant $|-\rangle$ population of states as compared to the sharp decay of Figure 5(d) and (e). This transient effect of entanglement between emitters embedded within a rolled-up zero-index waveguide is due to decoherence which is attributed to radiation losses and depopulation of emitters in the excited states [16]. To attain a steady entangled state $C(t \to \infty)$, it is relevant to compensate for the depopulation of the excited states by pumping the qubits with an external source. It is also interesting to note that to achieve strong steady-state entanglement between the qubits, the pump strength should not be too large; otherwise, strong interactions between the pump and the qubits as well as the pump and the zero-index channel may occur. This could eventually lead to qubit decoupling and lasing or strong resonances which may affect the decay channel of the emitter embedded within the waveguide channel [18]. In the current case, we utilized a weak pumping scenario and considered the effect of the pump on the zero-index waveguide negligible. We used pump intensities optimal to compensate for the depopulation of emitters in the excited states to enhance long-range entangled states.

We also assume a detuning parameter, $\Delta_i = \omega_0 - \omega_p = 0$, by utilizing an external source with a resonance frequency ω_p similar to the transition frequency ω_0 of the quantum emitters embedded in the rolled-up zero-index waveguide. Figure 6(a)–(c) shows the heatmap of the steady-state concurrence as a function of varied normalized Rabi frequencies Ω_1/γ for a single pump with the second pump kept constant ($\Omega_2/\gamma = 0$). We present here the steady entangled states at different interatomic distances $r_{12}/\lambda_0 = 0.5$, $r_{12}/\lambda_0 = 1.0$, and $r_{12}/\lambda_0 = 1.5$, respectively. The heatmap shows a high concurrence at $r_{12}/\lambda_0 = 0.5$ which corresponds to the high decay ratio γ_{12}/γ and minimal dipole-dipole interaction g_{12} which satisfy the aforementioned criteria for qubits entanglement. It can be seen that as the decay ratio γ_{12}/γ decreases relative to the interatomic distances r_{12}/λ_0, the concurrence decreases. Note that the normalized interatomic distance $r_{12}/\lambda_0 = 0.5$, $r_{12}/\lambda_0 = 1.0$, and $r_{12}/\lambda_0 = 1.5$ correspond to a qubit separation of $r_{12} = 725$ nm, $r_{12} = 1450$ nm, and $r_{12} = 2175$ nm, respectively, which exceeds the resonance energy transfer of quantum emitters in vacuum.

Figure 6(d)–(f) also shows the concurrence of quantum emitters in the presence of a coherent pump source at three normalized interatomic distances $r_{12}/\lambda_0 = 0.5$, $r_{12}/\lambda_0 = 1.0$, $r_{12}/\lambda_0 = 1.5$. Similar calculations for vacuum
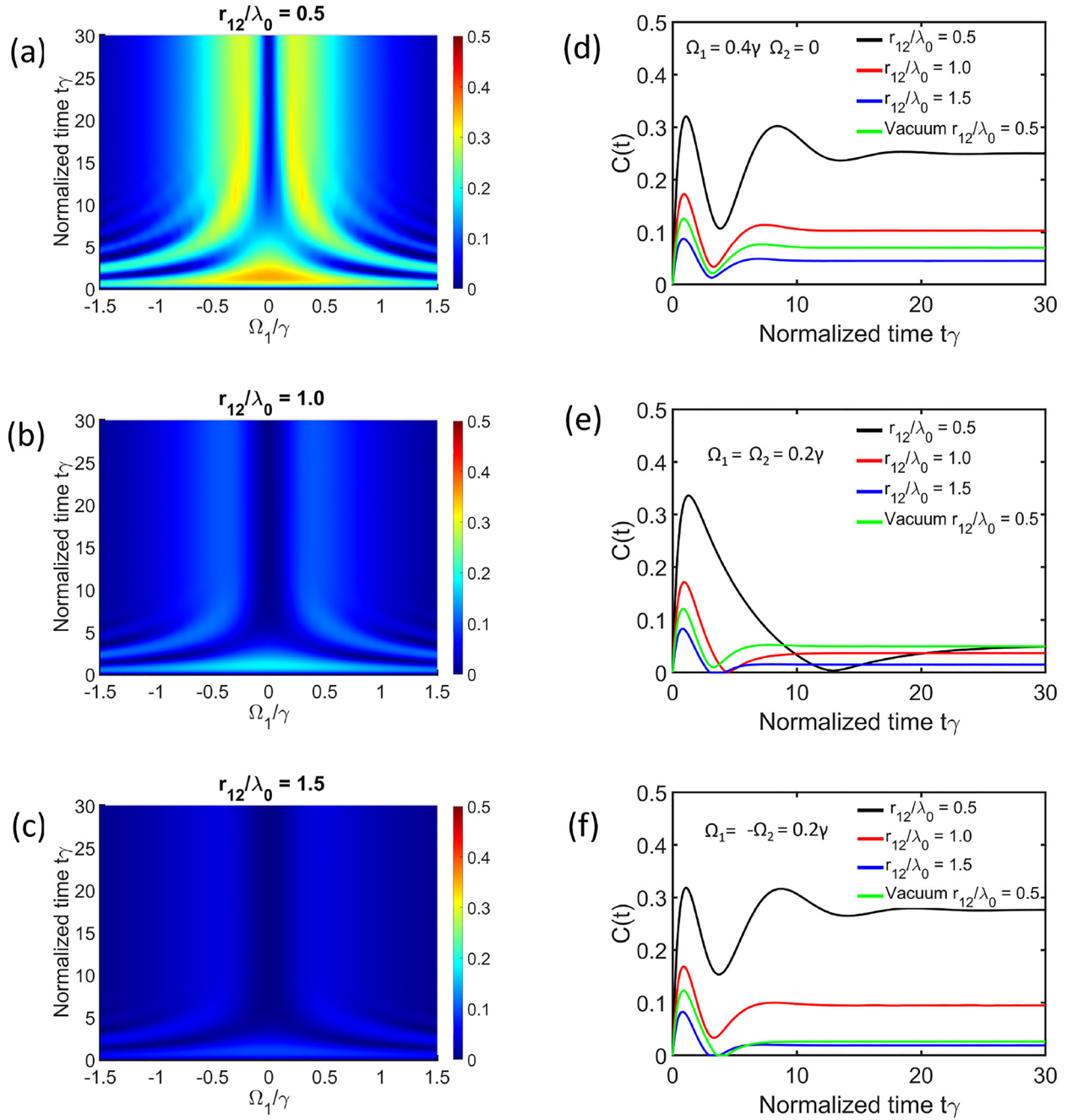
Figure 6: Persistent time dependent concurrence as a function of an external coherent source. The time dependent concurrence for different Rabi frequencies Ω_1/γ of a single pump source ($\Omega_2/\gamma = 0$) for different normalized interatomic distances (a) $r_{12}/\lambda_0 = 0.5$, (b) $r_{12}/\lambda_0 = 1.0$, and (c) $r_{12}/\lambda_0 = 1.5$. Time dependent concurrence between two quantum emitters at different normalized interatomic distances for different external pumping (d) asymmetric ($\Omega_1 = 0.4\gamma, \Omega_2 = 0$), (e) symmetric ($\Omega_1 = \Omega_2 = 0.2\gamma$), and (f) antisymmetric ($\Omega_1 = -\Omega_2 = 0.2\gamma$). Similar plot of the homogeneous medium is illustrated by the plot legend vacuum $r_{12}/\lambda_0 = 0.5$

reservoir ($r_{12}/\lambda_0 = 0.5$) (see Supplementary for details) are illustrated in the corresponding figures for reference purposes. We implement three types of pumps namely, asymmetric with Rabi frequencies $\Omega_1 \neq 0, \Omega_2 = 0$, symmetric with $\Omega_1 = \Omega_2$, and antisymmetric pumping with Rabi frequencies $\Omega_1 = -\Omega_2$. As expected, we obtain high

steady-state concurrence at $r_{12}/\lambda_0 = 0.5$ to $r_{12}/\lambda_0 = 1.0$, as compared to the vacuum medium. This shows that the zero-index rolled-up waveguide attains high entangled states at the cutoff wavelength and enhance long-range interactions of quantum emitters. From all the aforementioned pumping states, we see a persistent concurrence as a result of

the external source which compensates for the depopulation of the entangled states. Figure 6(d) and (f) (i.e., asymmetric and antisymmetric pumping) show quite identical steady-state concurrence with high entangled states in the proposed zero-index rolled-up waveguide at different interatomic distances r_{12}/λ_0. In addition, the symmetric pumping criteria sustains the concurrence to normalized time $t\gamma = 15$ at $r_{12}/\lambda_0 = 0.5$. The high and persistent concurrence for the different pumping criteria (i.e., asymmetric and antisymmetric pumping) illustrates that one can achieve steady entangled states $C(t \to \infty)$ by compensating for the depopulation of the excited states through pumping of the qubits with a coherent external source (i.e., monochromatic laser source).

5 Conclusions

We have presented an alternate, more practical, and experimentally attainable rolled-up zero-index waveguide using a unique self-rolling mechanism. Based on the parameters attained experimentally, we implemented numerical methods to study the photonic properties of the rolled-up zero-index waveguide. The numerical calculations demonstrate that, at the cutoff wavelength, the rolled-up zero-index waveguide can serve as a reservoir to mediate dipole-dipole interactions and long-range entangled states. Moreover, the calculations establish that the rolled-up zero-index waveguide design will enhance resonance energy transfer and transient entanglement of qubits at the cutoff wavelength. We also demonstrate that the transient entanglement of qubits mediated by this novel rolled-up zero-index waveguide could reach its steady-state by using an external pump source. The different pumping systems compensate for the depopulation of the emitter excited states in the rolled-up zero-index waveguide. Our design and numerical calculations have established the feasibility of the rolled-up zero-index waveguide to serve as a unique reservoir for quantum entanglement. The practical realization of the proposed design is also experimentally novel and relevant to pursue in our subsequent works. We also envision that this rolled-up zero-index waveguide could overcome the practical challenges of quantum emitters integration. This will open a new avenue to explore entanglement in zero-index mediums practically, which is promising for quantum teleportation, computing, and communication.

Supporting information available

The version of the codes used to generate the transient entanglement calculations are provided here: link (i.e., https://github.com/issahi62/Rolled-up-ENZ-Waveguide) and users of this code are kindly requested to cite its use in their work. Supplementary Information (SI) includes Entanglement theory of qubits coupled with a rolled-up zero-index waveguide, Unbounded vacuum dipole-dipole coupling and decay rate, Modelling, and Fabrication.

References

[1] Y. Liu and X. Zhang, "Metamaterials: a new Frontier of science and technology," *Chem. Soc. Rev.*, vol. 40, pp. 2494–2507, 2011.

[2] R. W. Ziolkowski and N. Engheta, *Metamaterials: Physics and Engineering Explorations*, Hoboken, NJ, John Wiley & Sons, 2006.

[3] M. Kadic, G. W. Milton, M. van Hecke, and M. Wegener, "3D metamaterials," *Nat. Rev. Phys.*, vol. 1, pp. 198–210, 2019.

[4] V. M. Shalaev, W. Cai, U. K. Chettiar, et al., "Negative index of refraction in optical metamaterials," *Opt. Lett.*, vol. 30, p. 3356, 2005.

[5] C. M. Soukoulis and M. Wegener, "Past achievements and future challenges in the development of three-dimensional photonic metamaterials," *Nat. Photonics*, vol. 5, pp. 523–530, 2011.

[6] R. Sokhoyan and H. A. Atwater, "Quantum optical properties of a dipole emitter coupled to an ϵ-near-zero nanoscale waveguide," *Opt. Express*, vol. 21, p. 32279, 2013.

[7] J. Ren, T. Wu, and X. Zhang, "Multifrequency multi-qubit entanglement based on plasmonic hot spots," *Sci. Rep.*, vol. 5, p. 13941, 2015.

[8] W. Ding, L. Y. Hsu, C. W. Heaps, and G. C. Schatz, "Plasmon-coupled resonance energy transfer II: exploring the peaks and dips in the electromagnetic coupling factor," *J. Phys. Chem. C*, vol. 122, pp. 22650–22659, 2018.

[9] P. K. Jha, N. Shitrit, J. Kim, X. Ren, Y. Wang, and X. Zhang, "Metasurface-mediated quantum entanglement," *ACS Photonics*, vol. 5, pp. 971–976, 2018.

[10] S. A. Biehs, V. M. Menon, and G. S. Agarwal, "Long-range dipole-dipole interaction and anomalous Förster energy transfer across a hyperbolic metamaterial," *Phys. Rev. B*, vol. 93, p. 245439, 2016.

[11] R. Loudon, *The Quantum Theory of Light*, New York, Oxford University Press, 1983.

[12] E. J. R. Vesseur, T. Coenen, H. Caglayan, N. Engheta, and A. Polman, "Experimental verification of n=0 structures for

visible light," *Phys. Rev. Lett.*, vol. 110, p. 013902, 2013.

[13] R. Fleury and A. Alù, "Enhanced superradiance in epsilon-near-zero plasmonic channels," *Phys. Rev. B Condens. Matter*, vol. 87, p. 201101[R], 2013.

[14] A. Gonzalez-Tudela, D. Martin-Cano, E. Moreno, L. Martin-Moreno, C. Tejedor, and F. J. Garcia-Vidal, "Entanglement of two qubits mediated by one-dimensional plasmonic waveguides," *Phys. Rev. Lett.*, vol. 106, p. 020501, 2011.

[15] I. D'Amico, D. G. Angelakis, F. Bussières, et al., "Nanoscale quantum optics," *Riv. Nuovo Cimento*, vol. 42, pp. 153−195, 2019.

[16] Y. Li, A. Nemilentsau, and C. Argyropoulos, "Resonance energy transfer and quantum entanglement mediated by epsilon-near-zero and other plasmonic waveguide systems," *Nanoscale*, vol. 11, pp. 14635−14647, 2019.

[17] S. A. H. Gangaraj, A. Nemilentsau, G. W. Hanson, and S. Hughes, "Transient and steady-state entanglement mediated by three-dimensional plasmonic waveguides," *Opt. Express*, vol. 23, p. 22330, 2015.

[18] S. A. H. Gangaraj, G. W. Hanson, and M. Antezza, "Robust entanglement with three-dimensional nonreciprocal photonic topological insulators," *Phys. Rev. A*, vol. 95, p. 063807, 2017.

[19] M. O. Scully and M. S. Zubairy, *Quantum Optics*, New York, Cambridge University Press, 1997.

[20] S. S. Islam, M. R. I. Faruque, and M. T. Islam, "An object-independent ENZ metamaterial-based wideband electromagnetic cloak," *Sci. Rep.*, vol. 6, p. 33624, 2016.

[21] B. C. Yildiz and H. Caglayan, "Epsilon-near-zero media coupled with localized surface plasmon modes," *Phys. Rev. B*, vol. 102, p. 165303, 2020.

[22] D. Martín-Cano, A. González-Tudela, L. Martín-Moreno, F. J. García-Vidal, C. Tejedor, and E. Moreno, "Dissipation-driven generation of two-qubit entanglement mediated by plasmonic waveguides," *Phys. Rev. B Condens. Matter*, vol. 84, p. 235306, 2011.

[23] Y. Li and C. Argyropoulos, "Controlling collective spontaneous emission with plasmonic waveguides," *Opt. Express*, vol. 24, p. 26696, 2016.

[24] D. Martín-Cano, L. Martín-Moreno, F. J. García-Vidal, and E. Moreno, "Resonance energy transfer and superradiance mediated by plasmonic nanowaveguides," *Nano Lett.*, vol. 10, pp. 3129−3134, 2010.

[25] A. W. Snyder and J. D. Love, *Optical Waveguide Theory*, London, Chapman and Hall, 1983.

[26] Y. Pan and S. Xu, "Energy tunnelling through an ultrasmall epsilon-near-zero channel in circular waveguide," *IET Microw., Antennas Propag.*, vol. 3, pp. 821−825, 2009.

[27] V. Prinz, V. Seleznev, A. Gutakovsky, et al., "Free-standing and overgrown InGaAs/GaAs nanotubes, nanohelices and their arrays," *Phys. E Low-dimens. Syst. Nanostruct.*, vol. 6, pp. 828−831, 2000.

[28] C. Strelow, S. Kietzmann, A. Schramm, et al, "AlInP-based rolled-up microtube resonators with colloidal nanocrystals operating in the visible spectral range," *Appl. Phys. Lett.*, vol. 101, p. 113114, 2012.

[29] P. B. Johnson and R. W. Christy, "Optical constants of the noble metals," *Phys. Rev. B*, vol. 6, pp. 4370−4379, 1972.

[30] E. Palik, *Handbook of Optical Constants of Solids*, Burlington, Academic Press, 1997.

[31] R. H. Dicke, "Coherence in spontaneous radiation processes," *Phys. Rev.*, vol. 93, pp. 99−110, 1954.

[32] E. Özgün, E. Ozbay, and H. Caglayan, "Tunable zero-index photonic crystal waveguide for two-qubit entanglement detection," *ACS Photonics*, vol. 3, pp. 2129−2133, 2016.

[33] E. Özgün and E. Ozbay, "Epsilon-near-zero waveguides for quantum information applications: a theoretical approach for n-qubits," *J. Phys. Soc. Jpn.*, vol. 87, p. 2129, 2018.

[34] J. Ren, T. Wu, B. Yang, and X. Zhang, "Simultaneously giant enhancement of Förster resonance energy transfer rate and efficiency based on plasmonic excitations," *Phys. Rev. B*, vol. 94, p. 125416, 2016.